Journal of Research in Ecology

An International Scientific Research Journal

ISSN No: Print: 2319 –1546; Online: 2319– 1554

Short Communication

Morphoradiation calculation and analysis: Case study-Bazman mountain-South East of Iran

Authors:
Abdollah Seif[1], Shahnaz Judaki[2] and Sina Solhi[3]

Institution:
1. Assistant Professor of Geomorphology, Department of Geographical Sciences and Planning, Isfahan University, Iran.

2. MA Graduated of Medical Geography, Isfahan University. Iran.

3. PhD student of Geomorphology, Isfahan University. Iran.

Corresponding author:
Abdollah Seif

ABSTRACT:

Morphoradition model has been used in this study to the modelling of rough surfaces and interfering earth topography and its relation with distribution of radiation energy. Global, direct, diffuse and duration of direct radiation are calculated through special days (Equinox, summer and winter solstice) and also for a whole year. Radiational map for each state resulted and then statistically analysed. Correlation between radiation and topographical factors were studied and analysed. Results showed that high elevation and slope lead to high variance of radiation values in all radiation types. At winter, sun shine is less than the other season's radiation variation and is more than other time. During winter days, radiation deference between north and south faced lands are increased. Diffused radiation has nearly no connection to topographical factors and variable, on the other hand direct and global radiation have more connection to topographical and morphological variations.

Keywords:
Radiation, Bazman mountain, Digital elevation model, Modeling.

Email ID:
solhi_sina@yahoo.com

Article Citation:
Abdollah Seif, Shahnaz Judaki and Sina Solhi
Morphoradiation calculation and analysis: Case study-Bazman mountain-South East of Iran
Journal of Research in Ecology (2017) 5(2): 958-974

Dates:
Received: 08 Mar 2017 **Accepted:** 11 June 2017 **Published:** 19 Aug 2017

Web Address:
http://ecologyresearch.info/documents/EC0368.pdf

Journal of Research in Ecology

INTRODUCTION

Solar radiation is the main source of energy in the earth and is the main factor that controls life and weather on earth. Solar energy determines pressure and humidity of earth through controlling temporal and spatial distribution and temperature of earth. Sun can be considered as a black body that continuously radiates. Total radiation energy of black body is calculated based on the Stefan Boltzmann law (Kaviani and Alijani, 2003).

The input energy into all natural and vital systems of earth planet is solar radiation energy and solar energy flow has created all morphogenic systems of earth surface. Accordingly, the importance of radiation energy in geomorphology science is determined. Distribution level of radiation energy on earth surface, which is originated from some factors including amount of solar radiation, the distance from the radiating source, latitude, axial rotation and orbital speed and uneven shapes such as slope, aspect and elevation, is the start point of changes and differences through earth surface (Solhi and Solhi 2014).

Accordingly, radiation differences would lead to temperature differences and distribution of globe temperature; global temperature effects on pressure changes on earth surface and these factors directly effect on winds breezing and would determine climate system of earth. Finally, climate system can incredibly control morphologic and erosional systems and determine the type of wind, water and glacial morphology and erosion in each place (Figure 1). Then, continuous changing loops of hydrologic and pedogenic systems are affected. The relevant studies to the radiation energy were evaluated based on natural morphologic systems and perspective of earth morphology due to the direct and indirect effects of this energy on human and human activities. Radiation energy as a new and clean energy can be used also to establish clean and without pollution on planets. This study has been conducted to estimate the radiation energy through a complete morphologic system with high accuracy since scientific morphologic communities have less considered uneven shape of the Earth or the same earth morph in their studies. (Seif *et al*., 2014).

Incident solar radiation at the earth's surface is the result of a complex interaction of energy between the atmosphere and the surface. Recently much progress

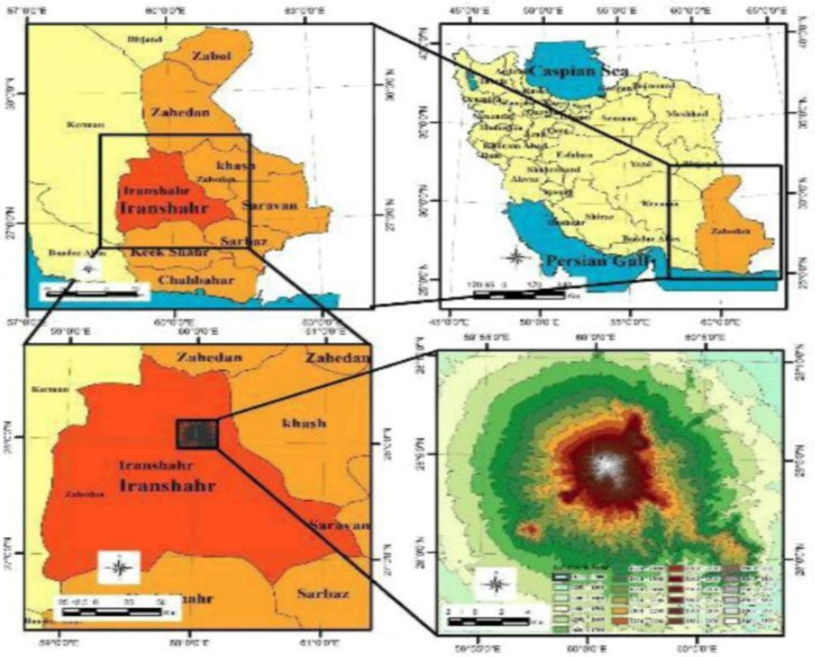

Figure 1. Location of study area- Bazman mountain (Southeast Iran)

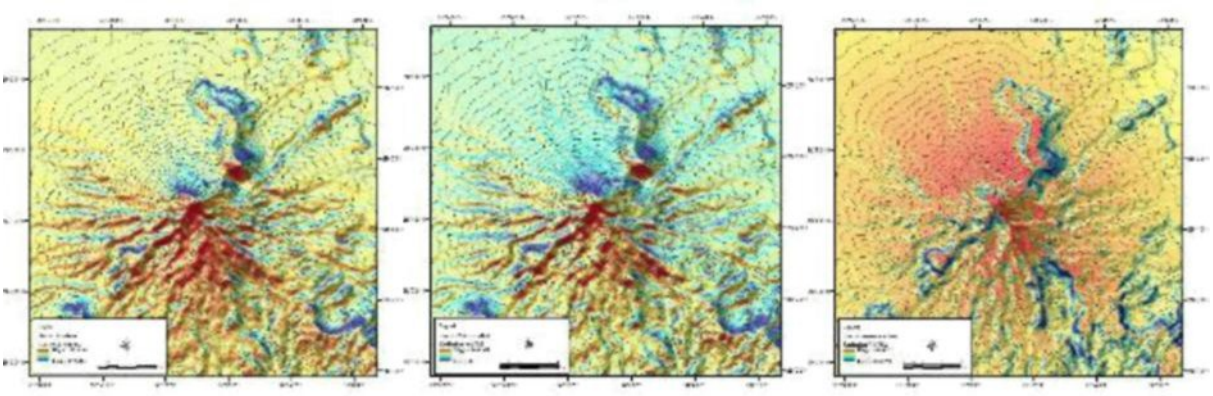

Figure 2. A. Direct radiation-equinox (2D); B. Direct radiation-winter solstice (2D); C. Direct radiation-summer solstice (2D)

has been made towards the creation of accurate, physically based solar radiation formulations that can model this interaction over topographic and other surfaces (such as plant canopies) for a large range of spatial and temporal scales (Dubayah and Rich, 1996).

Topography is a major factor in determining the amount of solar energy incident at a location on the earth's surface. Variability in elevation, slope, slope orientation (aspect), and shadowing, can create strong local gradients in solar radiation that directly and indirectly affect many biophysical processes such as primary production, air and soil heating, and energy and water balances (Geiger, 1965; Holland and Steyn, 1975; Gates 1980; Kirkpatrick and Nunez, 1980; Dubayah and Katwijk, 1992).

Although it has been recognized that topographic effects are important, until recently little has been done to incorporate them in a quantitative and systematic manner into a modeling environment (Rich and Weiss, 1991; Dubayah and Katwijk, 1992; Hetrick *et al*., 1993a, b; Saving *et al*., 1993).

Specifically, total solar radiation in the Northern Hemisphere is lowest on north-facing slopes; and on south-facing slopes in the southern hemisphere. This pattern results in lower air temperatures on pole-ward-facing slopes (Andrews, 1971; Evans, 1977), By contrast, equator-facing slopes receive high levels of total insolation. These results were significantly contrasting between the number of north and south-facing slopes and aspects in many areas globally (Evans, 1977).

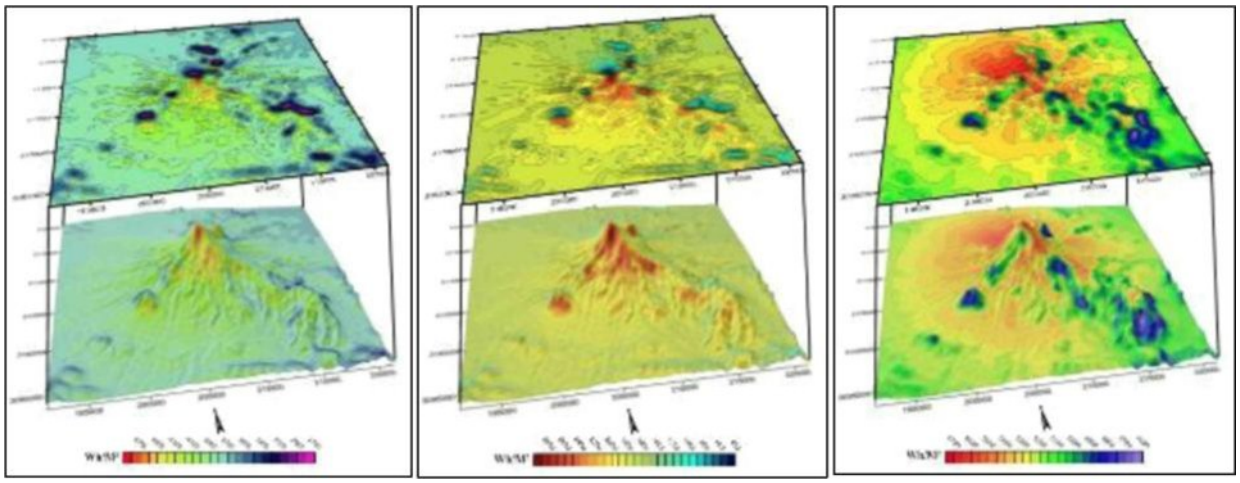

Figure 3. A. Direct radiation-equinox (3D); B. Direct radiation-winter solstice (3D); C. Direct radiation-summer solstice (3D) (Filtered by moving average technique-7×7 window size)

MATERIALS AND METHODS

The solar radiation analysis was calculated insolation across a landscape or for specific locations, based on the methods from the hemispherical view-shed algorithm developed by Rich (1994) and further extended by Fu and Rich (2000, 2002). The total amount of radiation calculated for a particular location or area is given as global radiation. The calculation of direct, diffuse, and global insolation are repeated for each feature location or every location on the topographic surface, producing insolation maps for an entire geographic area (Rich and Fu, 2000).

Solar radiation equations and calculations

Direct, diffuse, duration of direct radiation and global radiation are calculated here. Solar radiation is calculated for whole year and also three special days which these days are included as equinox, summer, winter and radiation solstice Table 1-4 (Fu, 2000).

Direct solar radiation

Total direct insolation (Dir_{tot}) for a given location is the sum of the direct insolation ($Dir_{\theta,\alpha}$) from all sun map sectors:

$$Dir_{tot} = \Sigma\, Dir_{\theta,\alpha} \quad (1)$$

The direct insolation from the sun map sector ($Dir_{\theta,\alpha}$) with a centroid at zenith angle (θ) and azimuth angle (θ) is calculated using the following:

$$Dir_{\theta,\alpha}=S_{const}\times\beta^{m(\theta)}\times SunDur_{\theta,\alpha}\times SunGap_{\theta,\alpha}\times Cos(AngIn_{\theta,\alpha}) \quad (2)$$

where, (S_{const}): the solar flux outside the atmosphere at the mean earth-sun distance, known as solar constant. The solar constant used in the analysis is 1367 w/m^2. This is

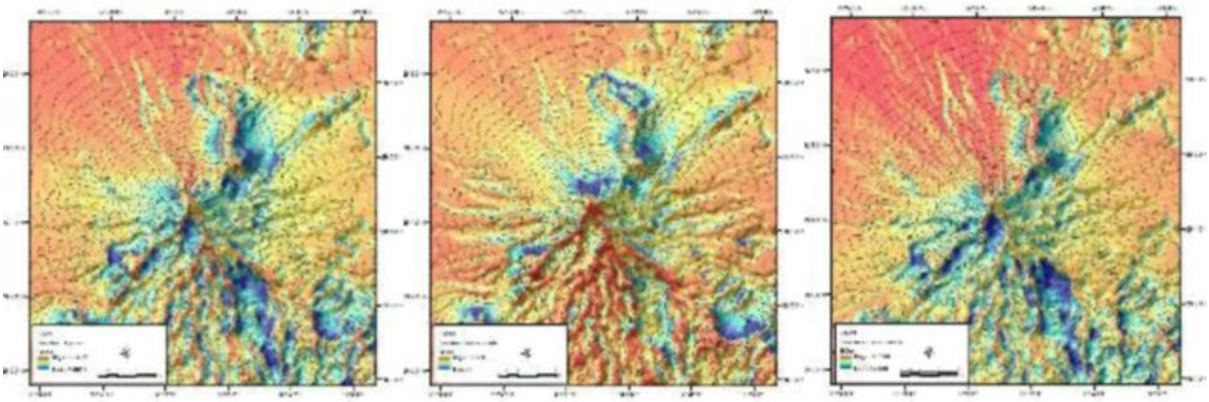

Figure 4. A. Duration-equinox (2D); B. Duration-winter solstice (2D); C. Duration-summer solstice (2D)

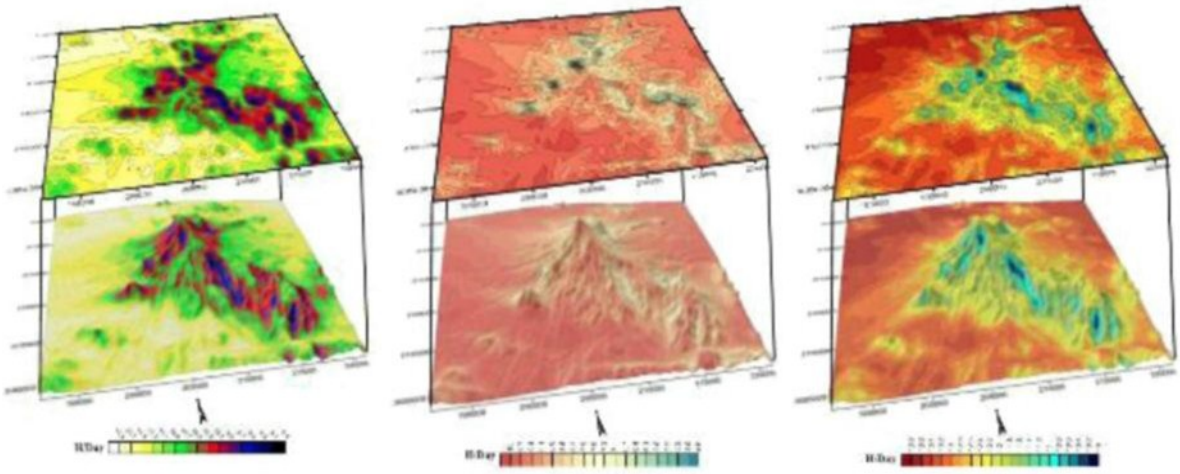

Figure 5. A. Duration-equinox (3D); B. Duration -winter solstice (3D); C. Duration-summer solstice (3D) (filtered by moving average technique -7×7 window size)

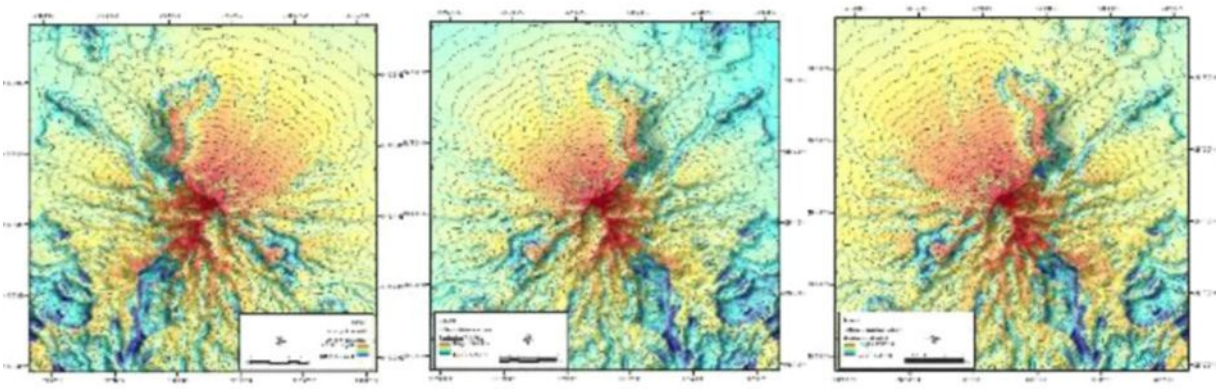

Figure 6. A. Diffuse radiation-equinox (2D); B. Diffuse radiation -winter solstice (2D); C. Diffuse radiation - summer solstice (2D)

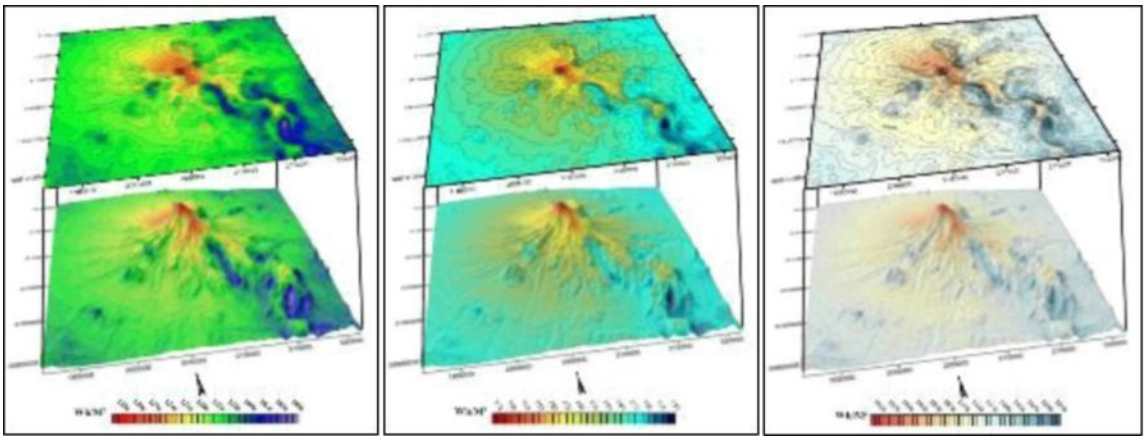

Figure 7. A. Diffuse radiation-equinox (3D); B. Diffuse radiation -winter solstice (3D); C. Diffuse radiation - summer solstice (3D) (filtered by moving average technique -7×7 window size)

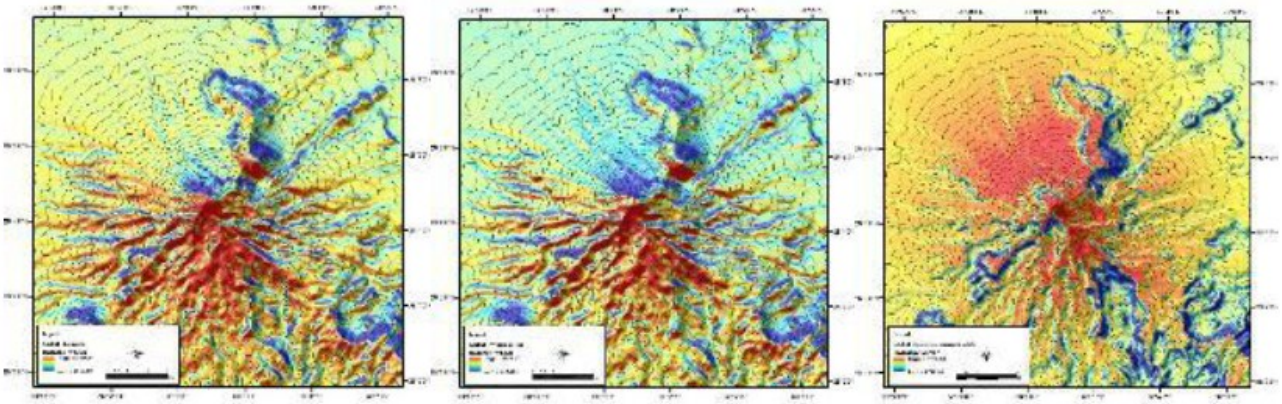

Figure 8. A. Global radiation-equinox (2D); B. Global radiation -winter solstice (2D); C. Global radiation - summer solstice (2D)

consistent with the World Radiation Centre (WRC) solar constant; β*:* The transmissivity of the atmosphere (averaged over all wavelengths) for the shortest path (in the direction of the zenith); mθ: The relative optical path length, measured as a proportion relative to the zenith path length (see equation 3); $SunDur_{\theta,\alpha}$: the time duration represented by the sky sector. For most sectors, it is equal to the day interval (for example, a month) multiplied by the hour interval (for example, a half hour) For partial sectors (near the horizon), the duration is calculated using spherical geometry; $SunGap_{\theta,\alpha}$: the gap fraction for the sun map sector; $AngIn_{\theta,\alpha}$: the angle of incidence between

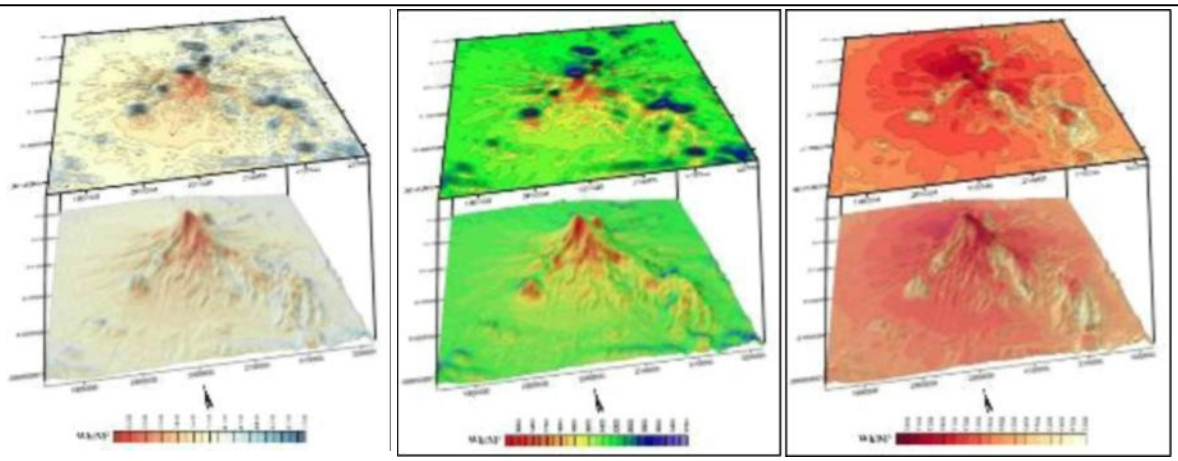

Figure 9. A. Global radiation-equinox (3D); B. Global radiation –winter solstice (3D); C. Global radiation - summer solstice (3D)

the centroid of the sky sector and the axis normal to the surface (see equation 4 below). Relative optical length, mθ, is determined by the solar zenith angle and elevation above sea level Table 5-10.

For zenith angles less than 80°, it can be calculated using the following equation:

$$m(\theta) = \frac{EXP\,(-0.000118 \times Elev - 1.638 \times 10^{-9} \times Elev^2)}{Cos_\theta} \qquad (3)$$

where, θ: The solar zenith angle; Elev: The elevation above sea level in meters.

The effect of surface orientation is taken into account by multiplying by the cosine of the angle of incidence. Angle of incidence ($AngInSky_{\theta,\alpha}$) between the intercepting surface and a given sky sector with a centroid at zenwith angle and azimuth angle is calculated using the following equation:

$$AngIn_{\theta,\alpha} = \text{acos}\,(\cos(\theta)) \times \text{Cos}(G_z) + \text{Sin}(\theta) \times \text{Sin}\,(G_z) \times \text{Cos}(\alpha - G_a) \quad (4)$$

where, G_z: The surface zenith angle. Note that for zenith angles greater than 80°, refraction is important; G_a: The surface azimuth angle.

Direct radiation of Bazman mountain based on Digital Elevation Model (DEM 30 m) is calculated for specific days (summer and winter solstice and equinox) and also whole year as which is shown in the Figure 2.

Duration of direct radiation

Duration of direct Radiation is calculated in this part Table 11-14. This is referred to the maximum time (in hour) that a pixel could be effected by sun radiation energy. This operation is calculated for daily (Special Days[4]) and yearly periods. Duration of direct radiation

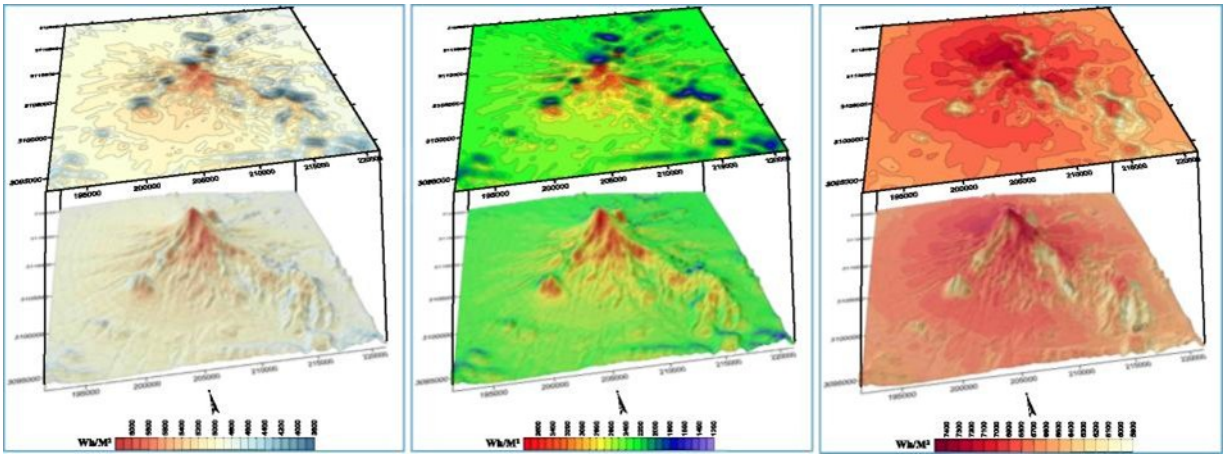

Figure 10. A. Global radiation-equinox (3D); B. global radiation -winter solstice (3D); C. global radiation - summer solstice (3D) (filtered by moving average technique -7×7 window size)

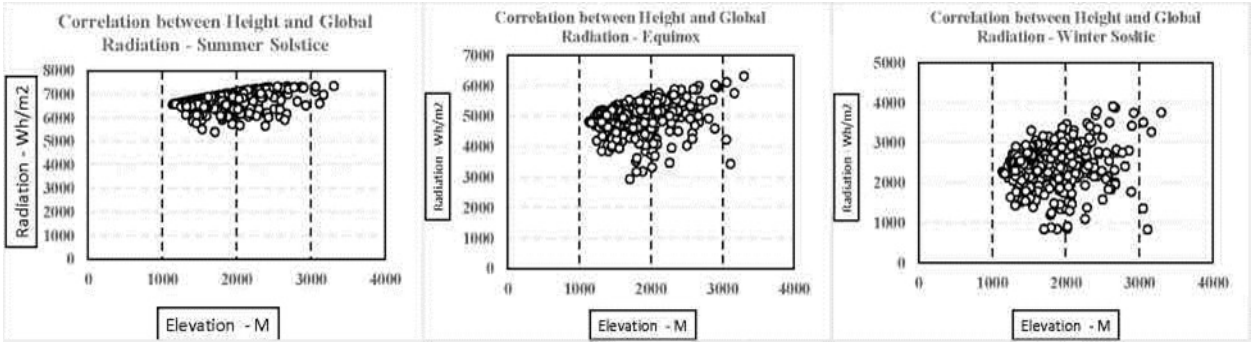

Figure 11. Height and global radiation correlation (specific days)

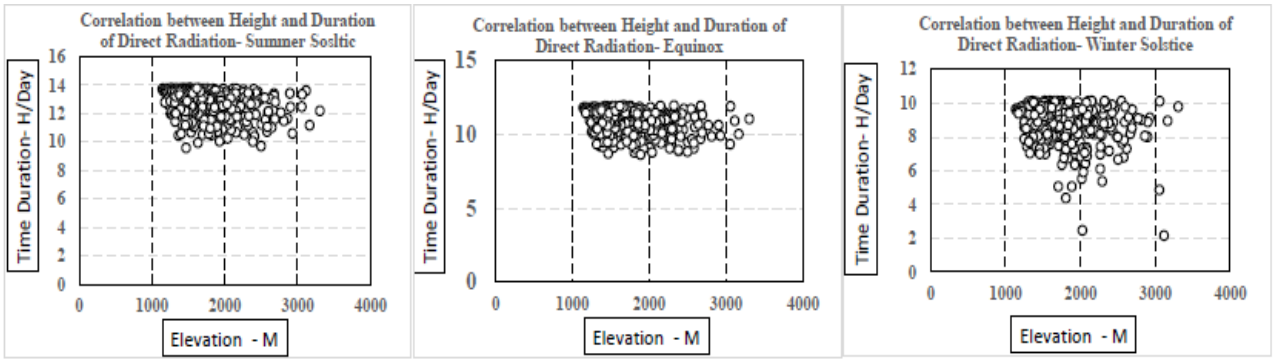

Figure 12. Height and duration of direct radiation correlations (specific days)

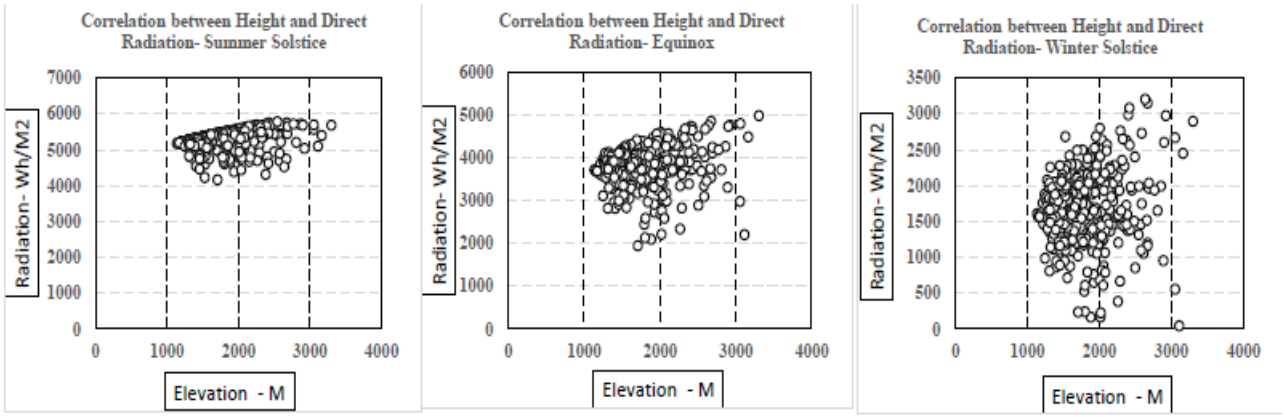

Figure 13. Height and direct radiation correlations (specific days)

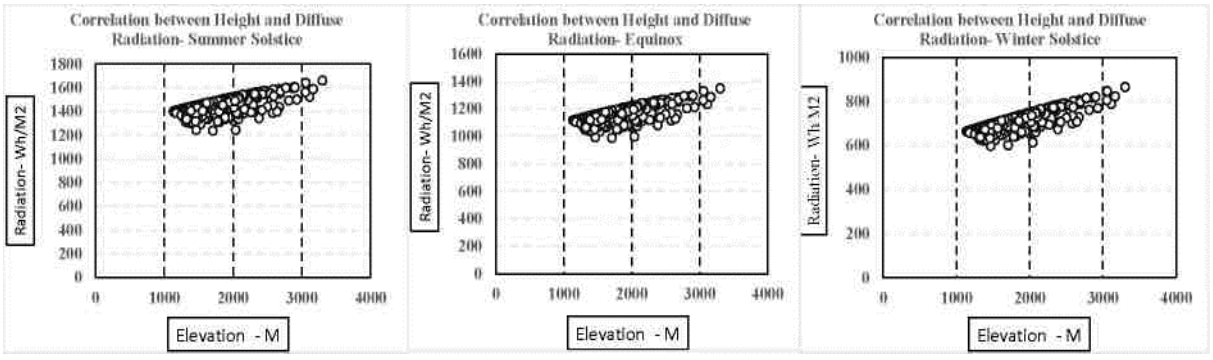

Figure 14. Height and diffuse radiation correlations (specific days)

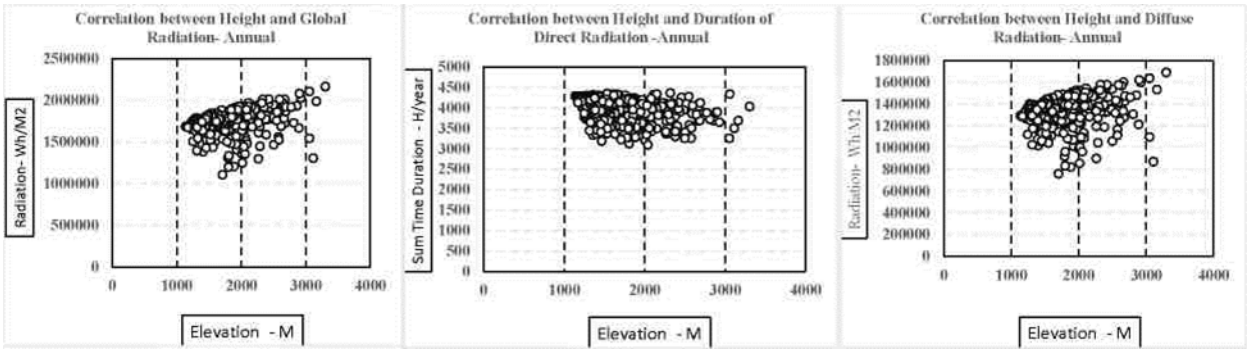

Figure 15. Height and diffuse, duration, global radiation correlations (annual)

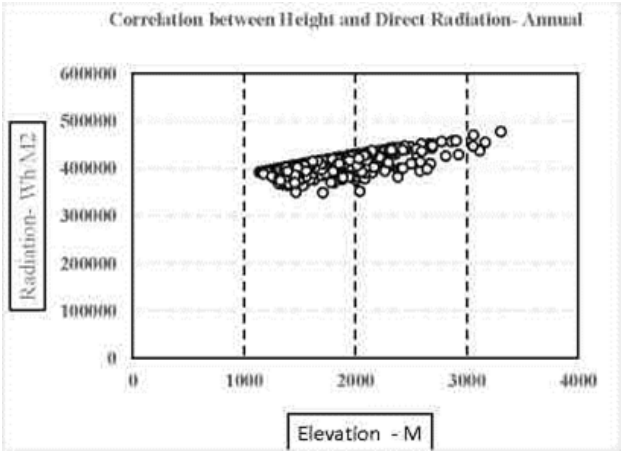

Figure 16. Height and direct radiation correlations (annual)

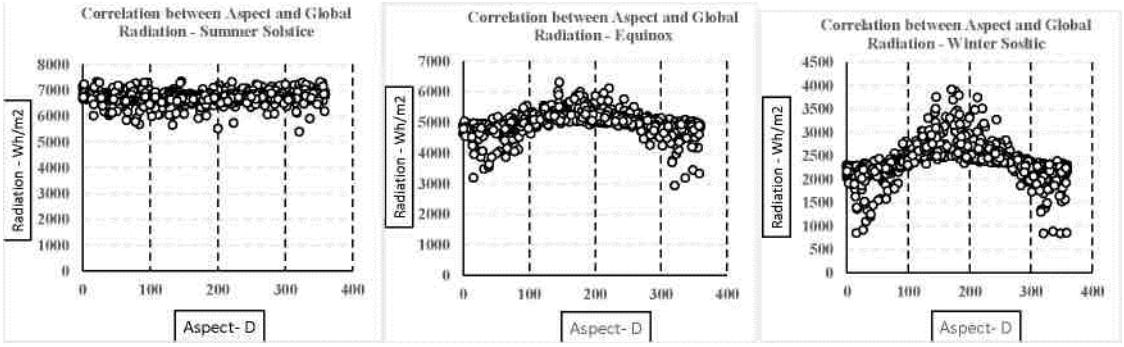

Figure 17. Aspect and global radiation correlations (specific days)

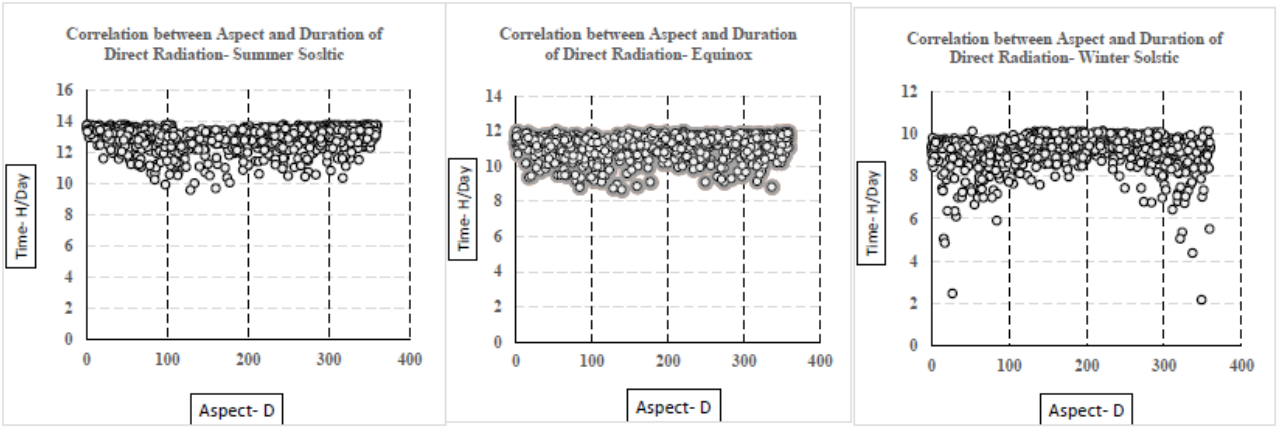

Figure 18. Aspect and duration of direct radiation correlations (specific days)

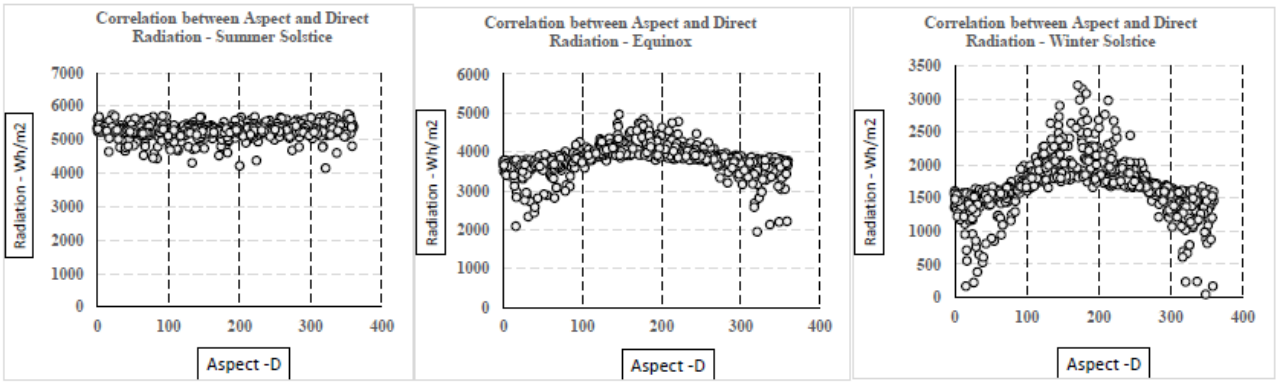

Figure 19. Aspect and direct radiation correlations (specific days)

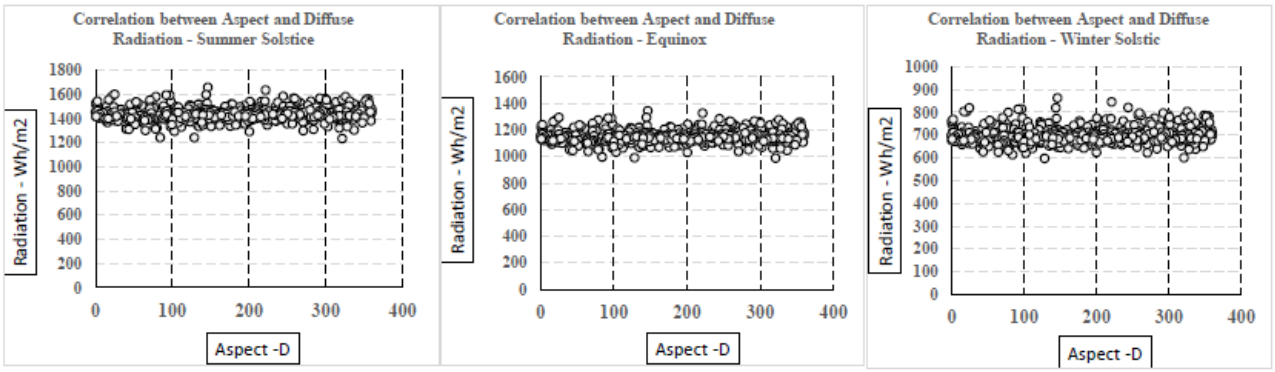

Figure 20. Aspect and diffuse radiation correlations (specific days)

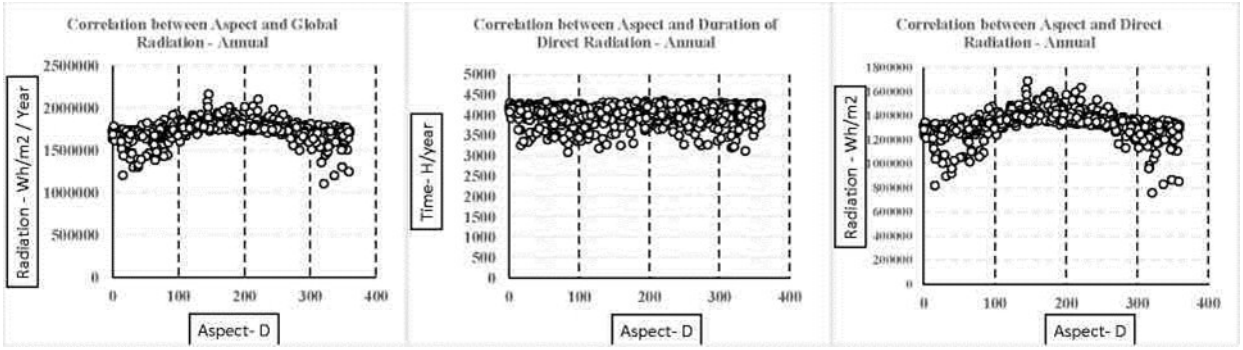

Figure 21. Aspect and duration of direct radiation, global, direct correlations (annual)

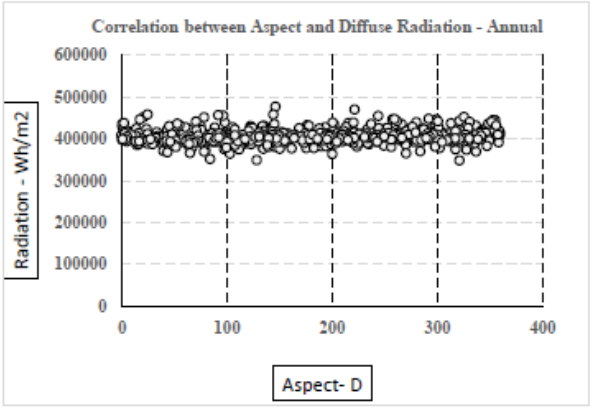

Figure 22. Aspect and direct radiation correlations (annual)

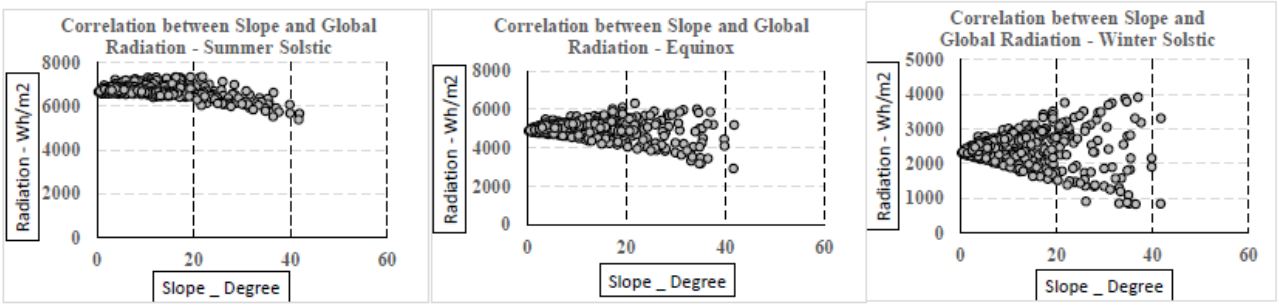

Figure 23. Slope and global radiation correlations (specific days)

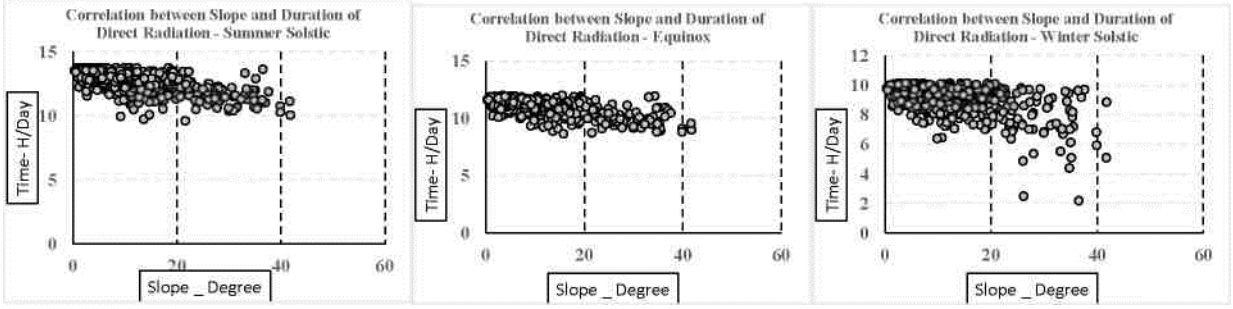

Figure 24. Slope and diffuse radiation correlations (specific days)

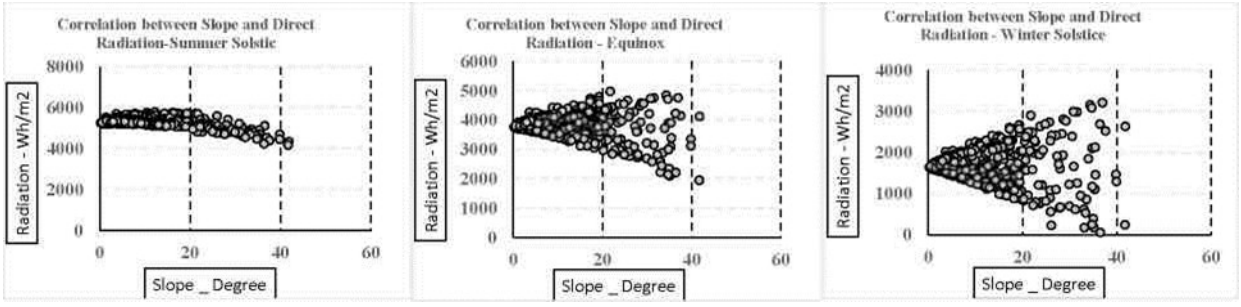

Figure 25. Slope and direct radiation correlations (specific days)

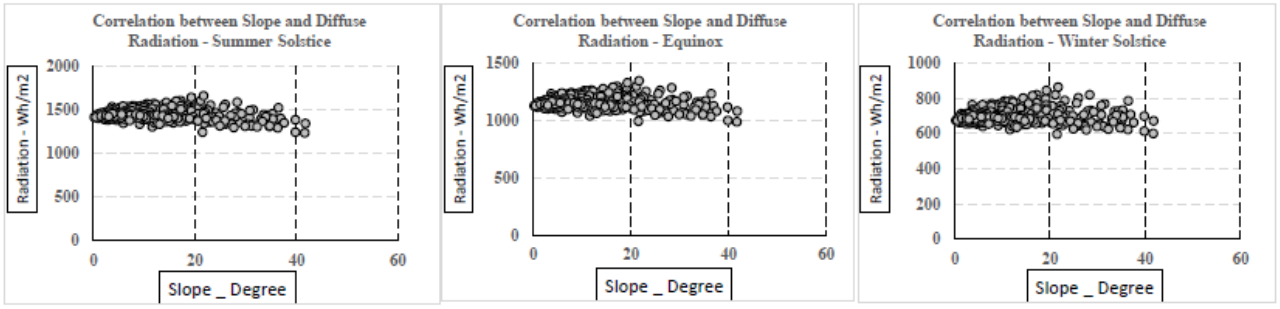

Figure 26. Slope and diffuse radiation correlations (specific days)

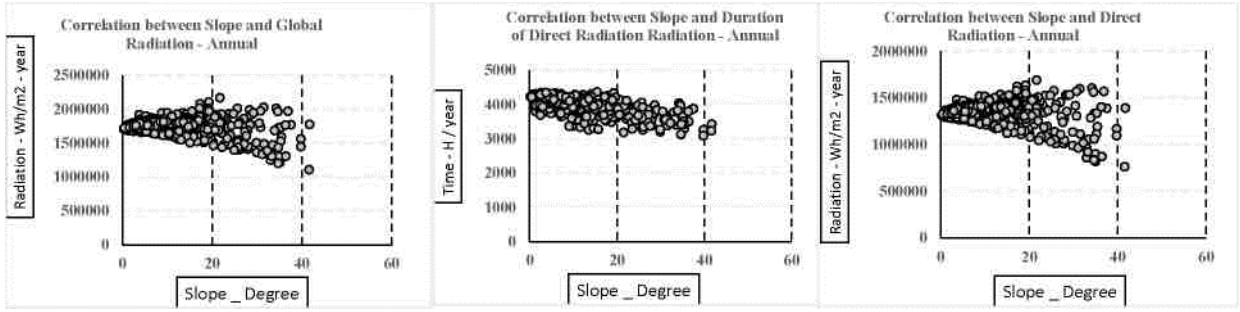

Figure 27. Correlations between slope and global, direct and duration of radiation (annual)

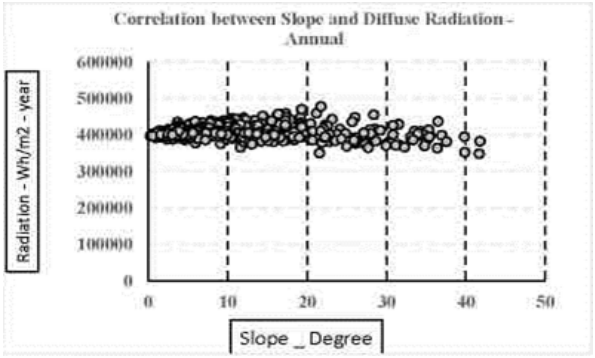

Figure 28. Correlations between slope and diffuse radiation (annual)

above Bazman mountain is calculated as shown in Figure 3-5.

Diffuse radiation calculation

For each sky sector, the diffuse radiation at its centroid (Dif) is calculated, integrated over the time interval, and corrected by the gap fraction and angle of incidence using the following equation:

$Dif_{\theta,\alpha}=R_{glb}\times P_{dif}\times Dur\times SkyGap_{\theta,\alpha}\times Weight_{\theta,\alpha}\times Cos(AngIn_{\theta,\alpha})$ (5)

where, R_{glb}: The global normal radiation (see equation 6 below); P_{dif}: The proportion of global normal radiation flux that is diffused. Typically it is approximately 0.2 for very clear sky conditions and 0.7 for very cloudy sky conditions; Dur: The time interval for analysis; $SkyGap_{\theta,\alpha}$: The gap fraction (proportion of visible sky) for the sky sector; $Weight_{\theta,\alpha}$: The proportion of diffuse radiation originating in a given sky sector relative to all sectors (see equations 7 and 8 below); $AngIn_{\theta,\alpha}$: The angle of incidence between the centroid of the sky sector and the intercepting surface.

The global normal radiation (R_{glb}) can be calculated by summing the direct radiation from every sector (including obstructed sectors) without correction for angle of incidence, then correcting for proportion of direct radiation, which equals $(1-P_{dif})$:

$$R_{glb}=\frac{(S_{Const}\ \Sigma(\beta^{m(\theta)}))}{(1-P_{dif})} \quad (6)$$

For the uniform sky diffuse model, $(Weight_{\theta,\alpha})$ is calculated as follows:

$$Weight_{\theta,\alpha}=\frac{(Cos\theta_2-Cos\theta_1)}{Div_{azi}} \quad (7)$$

where, (θ_1) and (θ_1): the bounding zenith angles of the sky sector; (Div_{azi}): the number of azimuthal divisions in the sky map.

For the standard overcast sky model, $(Weight_{\theta,\alpha})$

$$Weight_{\theta,\alpha}=\frac{(2Cos\theta_2+Cos2\theta_2-2Cos\theta_1-Cos2\theta_1)}{4\times Div_{azi}} \quad (8)$$

is calculated as follows:

Total diffuse solar radiation for the location (Dir_{tot}) is calculated as the sum of the diffuse solar radiation (Dif) from all the sky map sectors:

$Dir_{tot}=\Sigma Dir_{\theta,\alpha}$ 9

Diffuse Radiation of Bazman Mountain is calculated for specific days (summer and Winter Solstice and Equinox) and also whole year as which is shown in Figures 6 -9.

Global radiation calculation

Global radiation ($Global_{tot}$) is calculated as the sum of direct (Dir_{tot}) and diffuse (Dif_{tot}) radiation of all sun map and sky map sectors, respectively.

$Global_{tot}=Dir_{tot}+Dif_{tot}$

Spatial and distributional patterns of radiation

Distribution of radiation through elevation is analysed here. Correlation of topographic factors such as elevation, slope and aspect had studied and interpreted.

Elevation and radiation relationship

Elevation and radiation relationship had observed here.

Aspect and radiation relationship

The correlation between aspect and radiation parameters were studied here. We searched for a meaningful relationship between aspect variable and radiation variation.

Slope and radiation relationship

The connection between radiation and slope variation were studied here. And the results are shown in Figure 22. Table 17 is a correlation matrix that shows relationship between radiation and topographical factors.

Table 1. Direct radiation indices-summer solstice

S. No	Parameters	Value
1	Area	786.6 sq km
2	Perimeter	112.3 km
3	Min radiation	3572 Wh/m^2
4	Max radiation	6264 Wh/m^2
5	Average radiation	5294 Wh/m^2
6	Mode radiation	5263 Wh/m^2
7	Radiation standard deviation	185 Wh/m^2
8	Radiation max slope	85°
9	Radiation average slope	23°
10	Slope radiation standard deviation	23°

Table 2. Direct radiation indices-equinox

S. No	Parameters	Value
1	Area	786.6 sq km
2	Perimeter	112.3 km
3	Min radiation	722 Wh/m^2
4	Max radiation	5146 Wh/m^2
5	Average radiation	3805 Wh/m^2
6	Mode radiation	3770 Wh/m^2
7	Radiation standard deviation	311 Wh/m^2
8	Radiation max slope	86°
9	Radiation average slope	41°
10	Slope radiation standard deviation	22°

Table 3. Direct radiation indices-winter solstice

S. No	Parameters	Value
1	Area	786.6 sq km
2	Perimeter	112.3 km
3	Min radiation	0 Wh/m^2
4	Max radiation	3440 Wh/m^2
5	Average radiation	1676 Wh/m^2
6	Mode radiation	1580 Wh/m^2
7	Radiation standard deviation	341 Wh/m^2
8	Radiation max slope	85°
9	Radiation average slope	44°
10	Slope radiation standard deviation	22°

Table 4. Yearly direct radiation indices

S. No	Parameters	Value
1	Area	786.6 sq km
2	Perimeter	112.3 km
3	Min radiation	468722 wh/m^2
4	Max radiation	1737396 wh/m^2
5	Average radiation	1329930 wh/m^2
6	Mode radiation	1318482 wh/m^2
7	Radiation standard deviation	91503 wh/m^2
8	Radiation max slope	89.99°
9	Radiation average slope	89.47°
10	Slope radiation standard deviation	0.91°

Table 5. Duration of direct radiation indices-summer solstice

S. No	Parameters	Value
1	Area	786.6 sq km
2	Perimeter	112.3 km
3	Min duration	8.247 h
4	Max duration	13.751 h
5	Average duration	12.865 h
6	Mode duration	13.6 h
7	Standard deviation od duration	0.779 h
8	Max slope of duration	1.57°
9	Average slope of duration	0.14°
10	Standard deviation of slope duration	0.16°

Table 6. Duration of direct radiation indices-equinox

S. No	Parameters	Value
1	Area	786.6 sq km
2	Perimeter	112.3 km
3	Min duration	8.247 h
4	Max duration	13.751 h
5	Average duration	12.865 h
6	Mode duration	13.6 h
7	Standard deviation od duration	0.779 h
8	Max slope of duration	1.57°
9	Average slope of duration	0.14°
10	Standard deviation of slope duration	0.16°

Table 7. Duration of direct radiation indices- winter solstice

S. No	Parameters	Value
1	Area	786.6 sq km
2	Perimeter	112.3 km
3	Min duration	0 h
4	Max duration	10.131 h
5	Average duration	9.188 h
6	Mode duration	9.6 h
7	Standard deviation od duration	0.834 h
8	Max slope of duration	4.21°
9	Average slope of duration	0.16°
10	Standard deviation of slope duration	0.21°

Table 8. Yearly duration of direct radiation indices

S. No	Parameters	Value
1	Area	786.6 sq km
2	Perimeter	112.3 km
3	Min radiation	1761 wh/m^2
4	Max radiation	4365 wh/m^2
5	Average radiation	4029 wh/m^2
6	Mode radiation	4212 wh/m^2
7	Radiation standard deviation	240.197 wh/m^2
8	Radiation max slope	85.83°
9	Radiation average slope	28.76°
10	Slope radiation standard deviation	22.28°

Table 9. Diffuse radiation indices-summer solstice

S. No	Parameters	Value
1	Area	786.6 sq km
2	Perimeter	112.3 km
3	Min radiation	1107 wh/m^2
4	Max radiation	1739 wh/m^2
5	Average radiation	1441 wh/m^2
6	Mode radiation	1432 wh/m^2
7	Radiation standard deviation	47 wh/m^2
8	Radiation max slope	69.09°
9	Radiation average slope	6.86°
10	Slope radiation standard deviation	8.88°

Table 10. Diffuse radiation indices-equinox

S. No	Parameters	Value
1	Area	786.6 sq km
2	Perimeter	112 km
3	Min radiation	885 wh/m^2
4	Max radiation	1412 wh/m^2
5	Average radiation	1152 wh/m^2
6	Mode radiation	1143 wh/m^2
7	Radiation standard deviation	40.3 wh/m^2
8	Radiation max slope	64.73°
9	Radiation average slope	5.65°
10	Slope radiation standard deviation	7.51°

Table 11. Diffuse radiation indices-winter solstice

S. No	Parameters	Value
1	Area	786.6 sq km
2	Perimeter	112 km
3	Min radiation	536 wh/m^2
4	Max radiation	910 wh/m^2
5	Average radiation	698 wh/m^2
6	Mode radiation	685 wh/m^2
7	Radiation standard deviation	31.2 wh/m^2
8	Radiation max slope	53.33 wh/m^2
9	Radiation average slope	3.66°
10	Slope radiation standard deviation	5.06°

Table 12. Yearly diffuse radiation indices

S. No	Parameters	Value
1	Area	786.6 sq km
2	Perimeter	112.3 km
3	Min radiation	312184 wh/m^2
4	Max radiation	501189 wh/m^2
5	Average radiation	406251 wh/m^2
6	Mode radiation	403801 wh/m^2
7	Radiation standard deviation	14548 wh/m^2
8	Radiation max slope	89.92°
9	Radiation average slope	81.93°
10	Slope radiation standard deviation	9.64°

Table 13. Global radiation indices-summer solstice

S. No	Parameters	Value
1	Area	786.6 sq km
2	Perimeter	112.3 km
3	Min radiation	4720 wh/m^2
4	Max radiation	7998.841 wh/m^2
5	Average radiation	6735 wh/m^2
6	Mode radiation	6716 wh/m^2
7	Radiation standard deviation	225.82 wh/m^2
8	Radiation max slope	86.44°
9	Radiation average slope	25.03°
10	Slope radiation standard deviation	23.81°

Table 14. Global radiation indices-equinox

S. No	Parameters	Value
1	Area	786.6 sq km
2	Perimeter	112.3 km
3	Min radiation	1652 wh/m^2
4	Max radiation	6489 wh/m^2
5	Average radiation	4957 wh/m^2
6	Mode radiation	4964 wh/m^2
7	Radiation standard deviation	326 wh/m^2
8	Radiation max slope	87.19°
9	Radiation average slope	41.75°
10	Slope radiation standard deviation	22.78°

Table 15. Global radiation indices-winter solstice

S. No	Parameters	Value
1	Area	786.6 sq km
2	Perimeter	112.3 km
3	Min radiation	553 wh/m^2
4	Max radiation	4244 wh/m^2
5	Average radiation	2374 wh/m^2
6	Mode radiation	2320 wh/m^2
7	Radiation standard deviation	347 wh/m^2
8	Radiation max slope	86°
9	Radiation average slope	44°
10	Slope radiation standard deviation	347°

Table 16. Yearly global radiation indices

S. No	Parameters	Value
1	Area	786.6 sq km
2	Perimeter	112.3 km
3	Min radiation	795056 wh/m^2
4	Max radiation	2222641 wh/m^2
5	Average radiation	1736182 wh/m^2
6	Mode radiation	1722782 wh/m^2
7	Radiation standard deviation	98057 wh/m^2
8	Radiation max slope	89.99°
9	Radiation average slope	89.47°
10	Slope radiation standard deviation	0.95°

Table 17. Correlation matrix of radiation parameters based on Pearson method

Pearson Correlation	Elevation	Aspect	Slope	Hill shade	Global Summer Solstice	Global Equinox	Global Winter Solstice	Duration Summer Solstice	Duration Equinox	Duration Winter Solstice	Direct Summer Solstice	Direct Equinox	Direct Winter Solstice	Diffuse Summer Solstice	Diffuse Equinox	Diffuse Winter Solstice	Global - Yearly	Duration -Yearly	Direct - Yearly	Diffuse - Yearly
Elevation	1	.061	.596	-.001	.310	.245	.224	-.396	-.388	-.351	.227	.177	.159	.600	.658	.804	.288	-.411	.207	.677
Aspect	.061	1	-.074	.270	.143	.014	-.024	.112	.140	.070	.142	.000	-.034	.123	.121	.111	.028	.101	.012	.120
Slope	.596	-.074	1	-.217	-.523	-.182	.007	-.709	-.707	-.606	-.586	-.176	.000	-.189	-.123	.073	-.211	-.735	-.211	-.100
Hill shade	-.001	.270	-.217	1	.344	-.266	-.391	.188	.152	-.096	.369	-.301	-.411	.190	.178	.140	-.220	.068	-.262	.174
Global Summer Solstice	.310	.143	-.523	.344	1	.382	.111	.453	.425	.313	.993	.297	.047	.878	.856	.763	.471	.432	.378	.847
Global Equinox	.245	.014	-.182	-.266	.382	1	.958	-.028	.190	.581	.351	.994	.940	.454	.450	.425	.995	.293	.998	.448
Global Winter Solstice	.224	-.024	.007	-.391	.111	.958	1	-.189	.052	.513	.073	.973	.997	.250	.256	.265	.928	.161	.955	.257
Duration Summer Solstice	-.396	.112	-.709	.188	.453	-.028	-.189	1	.888	.510	.465	-.063	-.202	.337	.281	.108	.012	.878	-.026	.261
Duration Equinox	-.388	.140	-.707	.152	.425	.190	.052	.888	1	.705	.432	.165	.043	.335	.279	.108	.216	.966	.193	.260
Duration Winter Solstice	-.351	.070	-.606	-.096	.313	.581	.513	.510	.705	1	.311	.582	.516	.274	.226	.076	.581	.830	.591	.208
Direct Summer Solstice	.227	.142	-.586	.369	.993	.351	.073	.465	.432	.311	1	.272	.015	.816	.789	.688	.437	.435	.352	.779
Direct Equinox	.177	.000	-.176	-.301	.297	.994	.973	-.063	.165	.582	.272	1	.964	.355	.351	.327	.979	.271	.996	.349
Direct Winter Solstice	.159	-.034	.000	-.411	.047	.940	.997	-.202	.043	.516	.015	.964	1	.172	.176	.184	.903	.154	.940	.178
Diffuse Summer Solstice	.600	.123	-.189	.190	.878	.454	.250	.337	.335	.274	.816	.355	.172	1	.997	.958	.536	.356	.426	.995
Diffuse Equinox	.658	.121	-.123	.178	.856	.450	.256	.281	.279	.226	.789	.351	.176	.997	1	.977	.532	.297	.420	1.000
Diffuse Winter Solstice	.804	.111	.073	.140	.763	.425	.265	.108	.108	.076	.688	.327	.184	.958	.977	1	.501	.116	.390	.982
Global - Yearly	.288	.028	-.211	-.220	.471	.995	.928	.012	.216	.581	.437	.979	.903	.536	.532	.501	1	.316	.992	.529
Duration -Yearly	-.411	.101	-.735	.068	.432	.293	.161	.878	.966	.830	.435	.271	.154	.356	.297	.116	.316	1	.297	.276
Direct - Yearly	.207	.012	-.211	-.262	.378	.998	.955	-.026	.193	.591	.352	.996	.940	.426	.420	.390	.992	.297	1	.418
Diffuse - Yearly	.677	.120	-.100	.174	.847	.448	.257	.261	.260	.208	.779	.349	.178	.995	1.000	.982	.529	.276	.418	1

Legend

	Correlated at 0.05 level
	Correlated at 0.01 level
	Non correlated

Table 18. Radiation statistical index

	Elevation	Aspect	Slope	Hill shade	Global Summer Solstice	Global Equinox	Global Winter Solstice	Duration Summer Solstice	Duration Equinox	Duration Winter Solstice	Direct Summer Solstice	Direct Equinox	Direct Winter Solstice	Diffuse Summer Solstice	Diffuse Equinox	Diffuse Winter Solstice	Global - Yearly	Duration -Yearly	Direct - Yearly	Diffuse - Yearly
Sum	1336665	152665	7342	125148	5453110	4016322	1925293	10454	9046	7444	4285765	3083023	1359606	1167346	933300	565687	1406341730	3272211	1077264985	329076888
Minimum	1142	0	0	0	5389	2926	829	10	9	2	4155	1939	44	1234	987	597	1105040	3082	756894	348149
Maximum	3308	360	42	254	7340	6307	3910	14	12	10	5770	4962	3203	1658	1345	863	2164980	4355	1688070	476908
Range	2166	360	42	254	1951	3381	3080	4	3	8	1615	3023	3159	424	358	267	1059940	1273	931176	128759
Mean	1650	188	9	155	6732	4958	2377	13	11	9	5291	3806	1679	1441	1152	698	1736224	4040	1329957	406268
Median	1552	199	6	176	6739	4962	2350	13	11	9	5309	3807	1653	1439	1149	694	1739220	4115	1331690	405036
First quartile	1411	93	3	134	6652	4842	2242	13	11	9	5236	3704	1547	1418	1132	680	1699500	3948	1299150	398616
Third quartile	1798	284	12	197	6845	5108	2518	13	12	10	5384	3948	1824	1462	1169	711	1781270	4210	1372520	412285
Standard error	12.06	3.74	0.28	2.30	8.20	12.26	13.00	0.03	0.02	0.03	6.79	11.69	12.75	1.66	1.42	1.10	3676.62	8.23	3433.56	511.29
95% confidence interval	23.68	7.33	0.56	4.52	16.10	24.06	25.52	0.05	0.04	0.06	13.33	22.94	25.03	3.27	2.78	2.16	7217.04	16.15	6739.92	1003.64
99% confidence interval	31.15	9.65	0.73	5.94	21.18	31.65	33.57	0.07	0.06	0.08	17.53	30.18	32.93	4.30	3.66	2.84	9492.87	21.25	8865.29	1320.13
Variance	117882	11310	65	4293	54499	121678	136895	1	0	1	37328	110651	131735	2243	1624	977	10949213330	54844	9549341378	211749627
Average deviation	257.21	93.50	6.15	50.42	153.74	222.96	244.76	0.59	0.50	0.60	123.95	213.09	240.80	32.92	28.25	22.28	66836.08	178.18	61946.02	10219.94
Standard deviation	343.34	106.35	8.09	65.52	233.45	348.82	369.99	0.77	0.65	0.88	193.20	332.64	362.95	47.36	40.30	31.26	104638.49	234.19	97720.73	14551.62
Coefficient of variation	0.21	0.56	0.89	0.42	0.03	0.07	0.16	0.06	0.06	0.10	0.04	0.09	0.22	0.03	0.03	0.04	0.06	0.06	0.07	0.04
Skew	1.56	-0.12	1.65	-1.18	-1.28	-1.13	-0.08	-1.39	-1.46	-2.77	-1.67	-1.18	-0.13	0.17	0.45	1.15	-1.19	-1.50	-1.32	0.55
Kurtosis	2.93	-1.27	2.48	0.50	5.13	5.90	3.90	1.89	1.86	12.63	6.27	5.86	3.90	2.98	2.95	3.29	6.19	2.03	6.34	2.96
Kolmogorov-Smirnov stat	0.14	0.08	0.17	0.17	0.13	0.15	0.13	0.14	0.15	0.16	0.15	0.15	0.12	0.09	0.09	0.10	0.14	0.14	0.15	0.09
Critical K-S stat, alpha=.10	0.04	0.04	0.04	0.04	0.04	0.04	0.04	0.04	0.04	0.04	0.04	0.04	0.04	0.04	0.04	0.04	0.04	0.04	0.04	0.04
Critical K-S stat, alpha=.05	0.05	0.05	0.05	0.05	0.05	0.05	0.05	0.05	0.05	0.05	0.05	0.05	0.05	0.05	0.05	0.05	0.05	0.05	0.05	0.05
Critical K-S stat, alpha=.01	0.06	0.06	0.06	0.06	0.06	0.06	0.06	0.06	0.06	0.06	0.06	0.06	0.06	0.06	0.06	0.06	0.06	0.06	0.06	0.06

Cells that were in yellow are correlated at 0.05 level. Cells in orange were correlated at 0.01 level and red cells were non-correlated Table 18.

RESULTS AND DISCUSSION

With respect to Figure 10. Global radiation and elevation hadn't any linear relationship, so the linear regression coefficient is low. Variance of global radiation are increasing from summer solstice into winter solstice Table 16. As what is seen in Figure 10, global radiation had a little increase with elevation increment. So it is expected that elevated area receives more global radiation energy at summer solstice. Duration of direct radiation is decreased from summer solstice to winter solstice. Variance and standard deviation of duration of direct radiation are increasing from summer to winter solstice (Figure 11). Direct radiation and elevation didn't show any linear correlation but variation of direct radiation related to elevation from summer to winter solstice have increased (Figure 12). Diffused radiation and elevation have semi-linear relationship which have increased with elevation increment. Variance and standard deviation is almost low (Figure 13). Based on Figure 14, annual global radiation and elevation didn't show any detectable and meaningful correlation.

Based on Figure 15, global radiation and aspect variation doesn't have any clear relationship in the summer but this correlation are increasing into winter solstice. With respect to these graphs, it is clear that there is a strong increment of global radiation around aspects 100 up 300 degree so south faced land received more global radiation energy levels. Connection between aspect and global radiation from summer to winter solstice is increasing. Distributional pattern of global radiation showed that south-faced (100-300 North Azimuth Degree) lands receive more radiation energy levels (Figure 16.) Aspect and direct radiation connections pattern is similar to global radiation so direct radiation and aspect variation had lowest correlation in summer and the highest correlation is observed during winter days (Figure 17 and 18). Diffused radiation and aspect variations had the lowest correlation so diffuse radiation that doesn't follow land slope and aspect (Figure 19). Annual radiation maps showed that global and direct radiation that during a year has strong correlation with aspect variation and south faced lands receive more energy levels. Diffuse and duration of direct radiation didn't show such relationships (Figures 20 and 21). As what is shown in Figure 22, global radiation variation had a clear increase toward steep lands and also these variations of global radiation have a growth from summer toward winter. Duration of direct radiation and slope variation doesn't showed a meaningful correlation but variance of duration of direct radiation is increasing toward lands with high slope value and also increasing from summer toward winter (Figure 23). Direct radiation and slope variations pattern is similar to global radiation pattern. Direct radiation had a weak decrease toward steeper lands. Direct radiation variation is also increasing toward steeper lands (Figure 24). Slope and diffuse radiation has not showed detectable correlation and slope variations had a little effect on diffused radiational changes (Figure 25). Steeper lands have more variances' rate in global and direct radiation but duration and diffuse radiation didn't show this variation (Figures 26-28.)

CONCLUSION

Correlation of radiation and aspect, slope and elevation variable increased from summer to winter solstice. This is related to sun angle during winter and summer. When sun shines at high altitudes, variation of radiation increases above topography and different aspects showed more differences. South-faced lands received noticeable higher energy levels. Diffuse radiation has less relationship with topographic parameters. Direct and global radiation has stronger correlation to topographic variables.

REFERENCES

Andrews JT. (1971). Quantitative analysis of the factors controlling the distribution of corrie glaciers in Okoa Bay, East Baffin Island: (with particular reference to global radiation). In: Morisawa, M. (Ed.), quantitative geo-morphology: some aspects and applications. Proceedings of the 2nd. Geomorphology Symposium, Binghamton, State University of New York, 223-241 p.

Dubayah R and Rich PM. (1996). GIS and environmental modeling: progress and research issues. GIS World Books. Fort Collins, Co. GIS-based solar radiation modeling. 129-134 p.

Dubayah R and Van Katwijk V. (1992). The topographic distribution of annual incoming solar radiation in the Rio Grande river basin. *Geophysical Research Letters,* 19(22): 2231-2234.

Evans IS. (1977). World-wide variations in the direction and concentration of cirque and glacier aspects. Geografiska Annaler: Series A, Physical Geography, 59 (3/4): 151–175.

Fu P. (2000). A geometric solar radiation model with applications in landscape ecology. Ph.D. Thesis, Department of Geography, University of Kansas, Lawrence, Kansas, USA.

Fu P and Rich PM. (2000). The solar analyst 1.0 manual. Helios Environmental Modeling Institute (HEMI), USA. 1-53.

Fu P and Rich PM. (2002). A geometric solar radiation model with applications in agriculture and forestry. *Computers and Electronics in Agriculture,* 37(1-3): 25-35.

Gates DM. (1980). Biophysical ecology. New York: Springer-Verlag.

Geiger RJ. 1965. The climate near the ground. Cambridge: Harvard University Press, 1-518 p.

Hetrick WA, Rich PM, Barnes FJ and Weiss SB. (1993a). GIS-based solar radiation flux models. Proceedings ASPRS 1993 Annual Conference, New Orleans, 3: 132-43.

Hetrick WA, Rich PM and Weiss SB. (1993b). Modeling insolation on complex surfaces. Proceedings of the Thirteenth Annual ESRI User Conference, 2: 447-458.

Holland PG and Steyn DG. (1975). Vegetational responses to latitudinal variations in slope angle and aspect. *Journal of Biogeography,* 2(3): 179-83.

Kaviani MR and Alijani B. (2003). Applied principles of hydro-meteorological, SAMT Pub, Tehran Seif.

Kirkpatrick JB and Nunez M. (1980). Vegetation-radiation relationships in mountainous terrain: eucalypt-dominated vegetation in the Ridson Hills, Tasmania. *Journal of Biogeography,* 7(2): 197-208.

Rich PM, Dubayah R, Hetrick WA and Saving SC. (1994). Using view shed models to calculate intercepted solar radiation: applications in ecology. American society for photogrammetry and remote sensing technical papers, 524–529.

Rich PM and Fu P. (2000). Topoclimatic habitat models. Proceedings of the Fourth International Conference on Integrating GIS and Environmental Modeling.

Rich PM and Weiss SB. (1991). Spatial models of microclimate and habitat suitability: Lessons from threatened species. Proceedings Eleventh Annual ESRI User Conference, Palm Springs, CA, 95-99 p.

Saving SC, Rich PM, Smiley JT and Weiss SB. (1993). GIS-based microclimate models for assessment of habitat quality in natural reserves. Proceedings ASPRS 1993 Annual Conference, New Orleans, 3: 319-30.

Solhi A and Solhi SM. (2014). Morphoradition analysis

western heights of Eghlid and its relationship with morphological changes. *Journal of Geography and Environmental Planning,* 25(4): 150-162.

Seif A, Bazvand A and Solhi S. (2014). Morphoradition of alvand heights and its relation with quaternary glacial effects. *Indian Journal of Fundamental and Applied Life Science,* 6(S2): 304-314.